# Direct Model Predictive Current Control Strategy of DC-DC Boost Converters

Petros Karamanakos, *Student Member, IEEE,* Tobias Geyer, *Senior Member, IEEE,*
and Stefanos Manias, *Fellow, IEEE*

*Abstract*—**A model predictive control (MPC) algorithm for dc-dc boost converters is proposed in this paper. The proposed control scheme is implemented as a current-mode controller. Two control loops are employed, with the inner loop being designed in the framework of MPC. Two different objective functions are formulated and investigated. The control objective, i.e. the regulation of the current to its reference, is achieved by directly manipulating the switch, thus a modulator is not required. As a prediction model, a hybrid model of the converter is used, which captures precisely the continuous and the discontinuous conduction modes. The proposed control strategy achieves very fast current regulation, while exhibiting only a modest computational complexity. Simulation and experimental results substantiate the effectiveness of the proposed approach.**

*Index Terms*—**Dc-dc converter, model predictive control (MPC), optimal control, current control, hybrid system.**

## I. Introduction

**T**HE control of power electronic converters constitutes a challenging task, due to their switched nonlinear (or hybrid) characteristic. The standard control approach is to average the continuous-time dynamics associated with the different modes of operation, and to linearize them about the operating point. A different approach is to directly address the hybrid nature of these converters, see e.g. [1].

Despite the extensive research done in this area, the control problem of hybrid systems still poses challenges. However, the emergence of fast microprocessors and recent theoretical advances in the control of hybrid systems enabled the application of model predictive control (MPC) [2], [3]—a control method that has been successfully used in the process industry for more than three decades—to the field of power electronics. During the last decade, MPC has been successfully applied to several power electronics topologies [4]–[11], including dc-dc converters.

For the latter, MPC has been typically used in its simplest form—namely as a dead-beat controller—for controlling the predominant dc-dc converter topologies, i.e. the buck, the boost and the buck-boost converter [12]–[16]. A more complex MPC strategy was introduced in [17], [18] for the buck, and in [19], [20] for the boost converter. The nonlinear dynamics

P. Karamanakos is currently with the Institute for Electrical Drive Systems and Power Electronics, Technische Universität München, 80333 Munich, Germany (e-mail: p.karamanakos@ieee.org).

T. Geyer is with ABB Corporate Research, 5405 Baden-Dättwil, Switzerland (e-mail: t.geyer@ieee.org).

S. Manias is with the Department of Electrical and Computer Engineering, National Technical University of Athens, 15780 Zografou, Athens, Greece (e-mail: manias@central.ntua.gr).
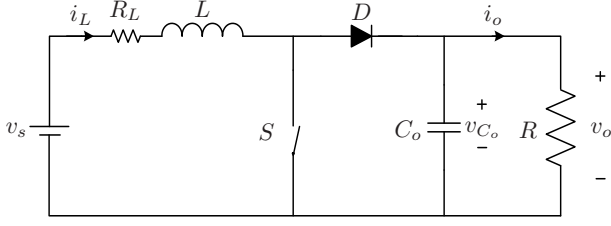
of the converter were approximated by a piecewise affine (PWA) model; the resulting controller regions were computed offline and stored in a look-up table, greatly reducing the computation time required to solve the control problem in real-time. In [21] an MPC approach based on numerical techniques was presented, and a sliding mode observer was designed, providing estimates of the varying voltage source and load resistor. In [22] the control problem of a full bridge dc-dc converter was formulated in the context of MPC in a computationally efficient manner. Finally, a current and a voltage MPC approach based on enumeration were introduced in [23] and in [24], respectively, where the control objectives were met by directly manipulating the switch.

This paper proposes a current-mode MPC scheme for the dc-dc boost converter, as in [25]. However, a more precise discrete-time model of the converter is introduced. In contrast to the aforementioned MPC-based approaches, this mathematical model, which serves as a prediction model for MPC, captures all operating modes of the inductor current, making it suitable for operation both in continuous (CCM) and discontinuous conduction mode (DCM). Hence, the converter state can be accurately predicted for the whole operating regime. Two control loops are employed. The outer loop adjusts the current reference for the inner loop such that the output voltage is regulated to its desired reference. The inner loop, posed in the MPC framework, drives the inductor current to its reference, by manipulating the switch. The outer loop is augmented by a Kalman filter, suitable for all operating modes. This state estimation scheme is designed so as to cope with all possible disturbances and uncertainties, which might arise from real-world non-idealities. To this end, the controller aims at rejecting all disturbances, including load and input voltage variations.

A major advantage of the current-mode MPC strategy introduced here is that only a short prediction horizon is needed, since the current exhibits a minimum-phase behavior with respect to the control input. In that way, the computational complexity, which is the dominant disadvantage of MPC, is decreased. Other benefits of the proposed scheme include the inherent robustness, the design simplicity, and the fast dynamics that MPC can provide. However, the absence of a modulator and the direct manipulation of the converter switches imply a variable switching frequency.

This paper is organized as follows. In Section II the hybrid continuous-time model of the converter is summarized. Furthermore, the discrete-time model suitable for the controller

Fig. 1. Topology of the dc-dc boost converter.



Fig. 2. The shape of the inductor current reveals the operation mode: the converter operates in CCM from $t$ to $t + T_s$, and in DCM from $t + T_s$ to $t + 2T_s$.

design is derived. Section III is devoted to the formulation of the constrained optimal control problem. In Section IV simulation results are given, and in Section V the experimental validation of the proposed control strategy is presented. Finally, in Section VI, conclusions are drawn.

## II. MATHEMATICAL MODEL OF THE BOOST CONVERTER

### A. Continuous-Time Model

The dc-dc boost converter is a switch-mode converter that is capable of producing a dc output voltage greater in magnitude than the dc input voltage. Fig. 1 illustrates the circuit topology examined, where $S$ denotes the controllable switch, $D$ the passive switch, and $R_L$ is the internal resistor of the inductance $L$, which, together with the capacitance $C_o$, forms a low-pass filter.

The independent states of the converter are the inductor current and the output voltage across the output capacitor. The state vector is defined as $x(t) = [i_L(t) \; v_o(t)]^T$. The system is described by the following affine (linear plus offset) continuous-time state-space equations [26]

$$\frac{dx(t)}{dt} = \begin{cases} A_1 x(t) + B v_s(t) & S = 1 \\ A_2 x(t) + B v_s(t) & S = 0 \; \& \; i_L(t) > 0 \\ A_3 x(t) & S = 0 \; \& \; i_L(t) = 0 \end{cases} \quad (1)$$

where the matrices $A_1$, $A_2$, $A_3$ and $B$ are given by

$$A_1 = \begin{bmatrix} -\frac{R_L}{L} & 0 \\ 0 & -\frac{1}{C_o R} \end{bmatrix}, \quad A_2 = \begin{bmatrix} -\frac{R_L}{L} & -\frac{1}{L} \\ \frac{1}{C_o} & -\frac{1}{C_o R} \end{bmatrix},$$

$$A_3 = \begin{bmatrix} 0 & 0 \\ 0 & -\frac{1}{C_o R} \end{bmatrix}, \quad \text{and} \quad B = \begin{bmatrix} \frac{1}{L} & 0 \end{bmatrix}^T,$$

where $R$ is the load resistance. The converter can operate in CCM and DCM, depending on the value of the inductor current $i_L(t)$, see Fig. 2. CCM refers to the case where $i_L(t)$ is always positive regardless of the state of the controllable switch $S$ (first two equations in (1)). DCM means that the inductor current reaches zero ($i_L(t) = 0$) for some period of time during the switching cycle, when the switch is *off* (third equation in (1)).

The output of the system corresponds to the output voltage, i.e.

$$y(t) = Cx(t), \quad (2)$$
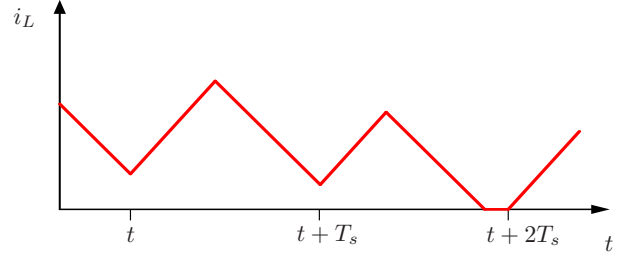
with $C = [0 \; 1]$.

### B. Modeling for Controller Design

The derivation of a discrete-time model suitable to serve as an internal prediction model for the controller is detailed in the following. The continuous-time equations of the model as given by (1) and (2) are discretized using the forward Euler approximation approach, resulting in the following discrete-time model of the converter:

$$x(k+1) = \begin{cases} E_1 x(k) + F v_s(k) & S = 1 \\ E_2 x(k) + F v_s(k) & S = 0 \; \& \; i_L(k+1) > 0 \\ E_3 x(k) & S = 0 \; \& \; i_L(k) = 0 \end{cases}$$

$$(3a)$$

$$y(k) = Gx(k), \quad (3b)$$

where $E_1 = \mathbf{1} + A_1 T_s$, $E_2 = \mathbf{1} + A_2 T_s$, $E_3 = \mathbf{1} + A_3 T_s$, $F = BT_s$, and $G = C$. Furthermore, $\mathbf{1}$ is the identity matrix and $T_s$ is the sampling interval.

However, as can be seen in Fig. 3, after the discretization the boost converter can operate in four different modes:

1) The inductor current is positive and the switch is *on* for the whole sampling interval, i.e. $i_L(k) > 0$, $i_L(k+1) > 0$ and $S = 1$.
2) The inductor current is positive and the switch is *off* for the whole sampling interval, i.e. $i_L(k) > 0$, $i_L(k+1) > 0$ and $S = 0$.
3) During the sampling interval the inductor current reaches zero, while the switch is *off*, i.e. $i_L(k) > 0$, $i_L(k+1) = 0$ and $S = 0$.
4) The inductor current is zero and the switch is *off* for the whole sampling interval, i.e. $i_L(k) = i_L(k+1) = 0$ and $S = 0$.

While (3) describes the modes "1", "2" and "4", it does not capture the transition from the CCM to DCM, i.e. mode "3". In order to derive a precise discrete-time mathematical model of the converter that captures all operating modes, the state-update given by (3a) is augmented by the additional equation

$$x(k+1) = E_{2,3} x(k) + \frac{\tau_1}{T_s} F v_s(k), \quad (4)$$

with $E_{2,3} = \frac{1}{T_s}(\tau_1 E_2 + \tau_2 E_3)$. Moreover, $\tau_1$ denotes the time-instant within the sampling interval, when the inductor current reaches zero, i.e. $i_L(k + \tau_1/T_s) = 0$, and $\tau_1 + \tau_2 = T_s$.

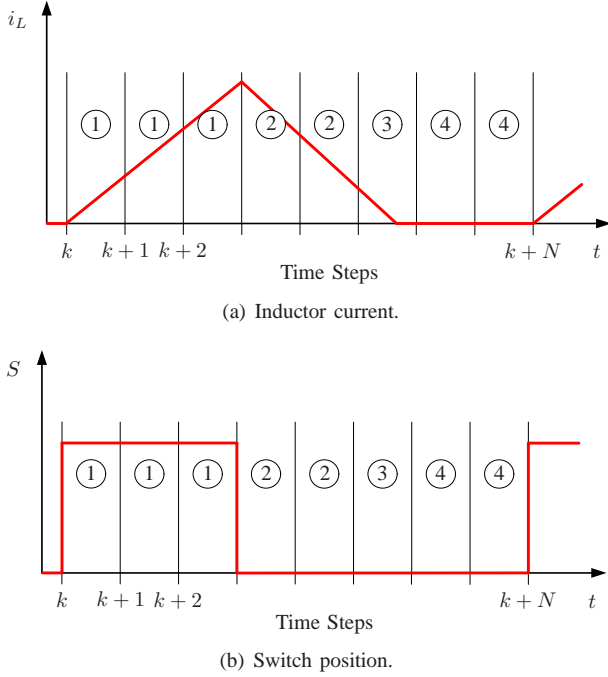(a) Inductor current.



(b) Switch position.

Fig. 3. Modes of operation of the boost converter: Depending on the shape of the current four different modes are introduced.
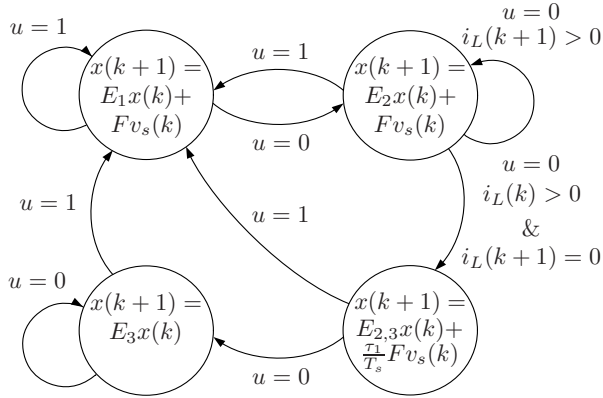


Fig. 4. Dc-dc converter represented as an automaton driven by conditions.

In Fig. 4 the operating modes of the converter are described. Mode transitions are specified by conditions, such as the switch position and the value of the current. To visualize the different modes and the transitions from one mode to the other, a binary variable $u$ denoting the switch position is introduced, where $u = 1$ refers to the switch $S$ being *on*, and $u = 0$ to the switch being *off* [27].

## III. CONTROL PROBLEM AND APPROACH

In this section, the design of the control scheme is presented. The MPC approach indirectly controls the output voltage by controlling the inductor current. This is achieved by appropriately manipulating the controllable switch. To derive the optimal sequence of control actions that minimizes a user-defined objective function subject to the plant dynamics, an enumeration technique is used.

### A. Model Predictive Control

MPC has established itself as a widespread controller thanks to its straight-forward design and implementation. An objective function needs to be chosen that captures the control objectives over the finite prediction horizon. At each sampling instant, the optimal solution is the sequence of control inputs that minimizes the objective function subject to the discrete-time model of the converter, resulting in the "best" predicted behavior of the system. The first element of this sequence is used as the process input. At the next step, new measurements or estimates are obtained, the horizon is shifted by one sampling interval and the optimization procedure is repeated. This strategy, known as *receding horizon policy* [2], [3], is employed in order to provide feedback.

### B. Control Objectives

The main control objective is to derive a switching strategy such that the inductor current is regulated along its reference trajectory. Furthermore, the closed-loop system needs to be robust to disturbances, i.e. the output voltage is to remain unaffected by changes in the input voltage and variations in the load.

### C. Objective Function

For the design of the objective function the deviation of the predicted evolution of the variables of concern from the desired behavior, over the horizon $N$, is taken into consideration. The control input at time-instant $kT_s$ is obtained by minimizing that function over the optimization variable, which is the sequence of switching states over the horizon $U(k) = [u(k)\ u(k+1)\dots u(k+N-1)]^T$. The sequence $U^*$ that minimizes the objective function is the *optimal* solution; the first element of the sequence, denoted as $u^*(k)$, is applied to the converter, the remaining elements are discarded and the procedure is repeated at the successive sampling instant based on new acquired measurements.

An illustrative example of the predicted state—here the inductor current—and the sequence of the control actions, i.e. the switching state, is depicted in Fig. 5. Three candidate switching sequences are shown for the prediction horizon $N = 7$. Note that the current that corresponds to time-step $k$ is the measured one, while from $k+1$ to $k+N$ the currents are predicted, assuming the switching sequences shown in Fig. 5(b).

In the control method introduced here, the control problem is formulated as a current regulation problem, with the deviation of the inductor current from its reference defined as

$$i_{L,\text{err}}(k) = i_{L,\text{ref}} - i_L(k). \qquad (5)$$

In this work, two different objective functions are proposed that precisely describe the control problem. In the first approach, the average value of the current error is penalized, while in the second one the rms value of the current error is considered. This allows us to use a shorter prediction horizon.

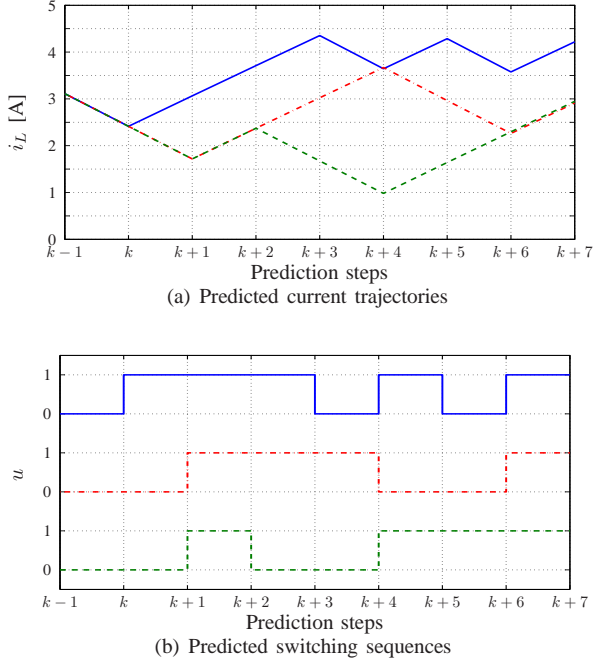In the following, the two alternative formulations of the objective function are described.

(a) Predicted current trajectories



(b) Predicted switching sequences

Fig. 5. Three candidate switching sequences for the prediction horizon $N = 7$.

*1) Average current error*: At time-step $k$, the average current error over the prediction interval $NT_s$ is given by:

$$i_{L,\text{err},avg}(k) = \frac{1}{NT_s} \int_{kT_s}^{(k+N)T_s} |i_{L,\text{err}}(t|k)| dt. \quad (6)$$

Exploiting the fact that the current slope changes only at the sampling instants and that in between the sampling instants the slope remains effectively constant[1], the above integral can be rewritten as:

$$i_{L,\text{err},avg}(k) = \frac{1}{N} \sum_{\ell=k}^{k+N-1} |\bar{i}_{L,\text{err}}(\ell|k)| \quad (7)$$

with $\bar{i}_{L,\text{err}}(\ell|k) = \frac{i_{L,\text{err}}(\ell|k) + i_{L,\text{err}}(\ell+1|k)}{2}$.

Based on this, the objective function

$$J_{avg}(k) = \sum_{\ell=k}^{k+N-1} \frac{1}{N} |\bar{i}_{L,\text{err}}(\ell|k)| + \lambda |\Delta u(\ell|k)| \quad (8)$$

can be formulated. The second term in (8) penalizes the difference between two consecutive switching states

$$\Delta u(k) = u(k) - u(k-1). \quad (9)$$

This term is added to decrease the switching frequency and to avoid excessive switching. The weighting factor $\lambda > 0$ sets the trade-off between the inductor current error and the switching frequency. In [28] some guidelines for tuning the weighting factor are given. Furthermore, it should be noted

---

[1]Strictly speaking, the current slope is constant only for modes "1", "2" and "4". For mode "3", when the converter transitions from CCM to DCM, the slope is constant for $\tau_1$, while for $\tau_2$ it is zero. However, the error resulting from the approximation given by (7) is negligible.

that the switching frequency varies depending on the operating point of the converter. The sampling interval $T_s$ serves as an upper bound on the switching frequency, i.e. $f_{sw} < 1/(2T_s)$; regardless of the operating point, the switching frequency is lower than half the sampling frequency.

*2) RMS current error*: The rms value of the current error over the prediction interval is equal to

$$i_{L,\text{err},rms}(k) = \sqrt{\frac{1}{NT_s} \int_{kT_s}^{(k+N)T_s} \left(i_{L,\text{err}}(t|k)\right)^2 dt} \quad (10)$$

with the current error as given in (5). This expression is equivalent to

$$i_{L,\text{err},rms}(k) = \frac{2}{3N} \sum_{\ell=k}^{k+N-1} 2\left(\bar{i}_{L,\text{err}}(\ell|k)\right)^2 - \tilde{i}_{L,\text{err}}(\ell|k) \quad (11)$$

with $\tilde{i}_{L,\text{err}}(\ell|k) = \frac{i_{L,\text{err}}(\ell|k) \cdot i_{L,\text{err}}(\ell+1|k)}{2}$.

Based on (11) the objective function for the rms current error-based approach is formulated as

$$J_{rms}(k) = \sum_{\ell=k}^{k+N-1} \frac{2}{3N} \left(2\left(\bar{i}_{L,\text{err}}(\ell|k)\right)^2 - \tilde{i}_{L,\text{err}}(\ell|k)\right)$$
$$+ \lambda\left(\Delta u(\ell|k)\right)^2. \quad (12)$$

### D. Optimization Problem

Subsequently, for both approaches, an optimization problem is formulated and solved. The control input in both cases is obtained by minimizing the corresponding objective function—(8) or (12)—subject to the converter model at each sampling instant, i.e.

$$U^*(k) = \arg\min J_\dagger(k)$$
$$\text{subject to eqs. (3), (4)} \quad (13)$$

where $J_\dagger$ denotes the objective function to be minimized, which is either $J_{avg}$ or $J_{rms}$.

The optimization problem (13) is solved using an enumeration strategy. All possible combinations of the switching state ($u = 0$ or $u = 1$) over the prediction horizon $N$ are enumerated, yielding the so-called *switching sequences* $U$. There exist $2^N$ switching sequences. For each switching sequence, the evolution of the variables of concern is calculated using (3) and (4), and the objective function is evaluated. The switching sequence that results in the minimum cost is chosen as the optimal one, $U^*$.

### E. Outer Loop

The reference current for the inner loop is derived from the outer loop based on a feed-forward scheme, using the power balance equation $P_{in} = P_{out}$. Assuming that the power switches are ideal, the following expression for the desired current results:

$$I_{L,\text{des}} = \frac{V_s}{2R_L} - \sqrt{\left(\frac{V_s}{2R_L}\right)^2 - \frac{V_{o,\text{ref}}^2}{RR_L}}. \quad (14)$$

In the above equation small-ripple approximation is used [26], i.e. $v_s \approx V_s$ and $v_{o,\text{ref}} \approx V_{o,\text{ref}}$.

In order to further improve the transient response of the output voltage, a term proportional to the voltage error, i.e. $v_{o,\text{ref}} - v_o$, is added to (14). Hence, the reference inductor current is given by

$$I_{L,\text{ref}} = I_{L,\text{des}} + h(V_{o,\text{ref}} - v_o),  \quad (15)$$

with $h \in \mathbb{R}^+$. In (15) the small-ripple approximation is used again.

*F. Load Variations*

So far, the load has been assumed to be time-invariant and known. In the vast majority of the applications, however, this is not the case; the load typically varies in an unknown way, resulting in a model mismatch and therefore in a steady-state output voltage error. To overcome this, an additional external loop that provides state estimates needs to be designed. Moreover, this loop will adjust the current reference so as to remove the steady-state error between the inductor current and its reference.

Even though a PI-based loop might suffice to meet the two objectives mentioned above, in this work a discrete-time Kalman filter [29] is implemented, similar to [17]. Thanks to its integrating nature, the Kalman filter provides offset-free output voltage tracking, while not being operating point dependent.

The model of the converter given by (3) and (4) is augmented by two integrating disturbance states, $i_e$ and $v_e$, that model the effect of load variations on the inductor current and the output voltage, respectively. Hence, the Kalman filter estimates the augmented state vector

$$x_a = \begin{bmatrix} i_L & v_o & i_e & v_e \end{bmatrix}^T, \quad (16)$$

consisting of the measured state variables, $i_L$ and $v_o$, and the disturbance states. Starting from (3a) and (4), the stochastic discrete-time state equation of the augmented model is

$$x_a(k+1) = E_{za}x_a(k) + F_{za}v_s(k) + \xi(k) \quad (17)$$

with $z = \{1, 2, 3, 4\}$, corresponding to the four modes of operation.

The measurement equation is given by

$$x(k) = \begin{bmatrix} i_L(k) \\ v_o(k) \end{bmatrix} = G_a x_a(k) + \nu(k). \quad (18)$$

The matrices are

$$E_{1a} = \begin{bmatrix} E_1 & \mathbf{0} \\ \mathbf{0} & \mathbf{1} \end{bmatrix}, E_{2a} = \begin{bmatrix} E_2 & \mathbf{0} \\ \mathbf{0} & \mathbf{1} \end{bmatrix}, E_{3a} = \begin{bmatrix} E_{2,3} & \mathbf{0} \\ \mathbf{0} & \mathbf{1} \end{bmatrix},$$

$$E_{4a} = \begin{bmatrix} E_3 & \mathbf{0} \\ \mathbf{0} & \mathbf{1} \end{bmatrix}, F_{1a} = F_{2a} = \begin{bmatrix} F \\ 0 \\ 0 \end{bmatrix}, F_{3a} = \begin{bmatrix} \frac{\tau_1}{T_s}F \\ 0 \\ 0 \end{bmatrix},$$

$$F_{4a} = \begin{bmatrix} 0 & 0 & 0 & 0 \end{bmatrix}^T, \quad \text{and} \quad G_a = \begin{bmatrix} \mathbf{1} & \mathbf{1} \end{bmatrix}, \quad (19)$$

where $\mathbf{1}$ is the identity matrix of dimension two, and $\mathbf{0}$ are square zero matrices of dimension two. The process noise is denoted by $\xi \in \mathbb{R}^4$ and the measurement noise by $\nu \in \mathbb{R}^2$. Both of the noise disturbances represent zero-mean, white Gaussian noise sequences with normal probability distributions. The process noise covariance matrix is positive semi-definite and it is given by $E[\xi\xi^T] = Q$. The measurement noise covariance matrix is given by $E[\nu\nu^T] = R$, and it is positive definite.

Based on the augmented converter model (17), a switched discrete-time Kalman filter can be implemented. Since the state-update for each operating mode is different, the respective Kalman gains are different. Hence, four unique Kalman gains $K_z$, with $z = \{1, 2, 3, 4\}$, need to be calculated and implemented.

The state equation of the estimated augmented state $\hat{x}_a(k)$ is given by

$$\hat{x}_a(k+1) = E_{za}\hat{x}_a(k) + K_z G_a\big(x_a(k) - \hat{x}_a(k)\big) + F_{za}v_s(k). \quad (20)$$

The Kalman gains are calculated based on the noise covariance matrices, $Q$ and $R$. These matrices are chosen such that high credibility is assigned to the measurements of the physical states ($i_L$ and $v_o$), and low credibility to the dynamics of the disturbance states ($i_e$ and $v_e$). As a result, the Kalman filter provides estimates of the disturbances that can be used to remove their influence from the output voltage and inductor current. The estimated disturbance state $\hat{v}_e$ is used to adjust the output voltage reference $v_{o,\text{ref}}$

$$\tilde{v}_{o,\text{ref}} = v_{o,\text{ref}} - \hat{v}_e. \quad (21)$$

Hence, in (14) and (15) the *modified* voltage reference $\tilde{v}_{o,\text{ref}}$ is taken into consideration, instead of the given value $v_{o,\text{ref}}$.

Following the same procedure, the inductor current reference $i_{L,\text{ref}}$ is adjusted using the corresponding estimated disturbance state $\hat{i}_e$, i.e.

$$\tilde{i}_{L,\text{ref}} = i_{L,\text{ref}} - \hat{i}_e. \quad (22)$$

Moreover, the controller is based on the estimated states $\hat{v}_o$ and $\hat{i}_L$, rather than on the measured ones, $v_o$ and $i_L$.

*G. Control Algorithm*

The proposed control technique is summarized in Algorithm 1. The function $f_\dagger$ stands for the state-update given by (3), and $g_\dagger$ refers to the function that calculates the current error according to (7) or (11). For the average current error based approach, $p = 1$ is used, whilst for the rms current error based one, $p = 2$ is chosen. In Fig. 6 the control diagram of the proposed control strategy including both loops is depicted.

## IV. SIMULATION RESULTS

In this section simulation results are presented demonstrating the dynamical performance of the proposed controller. The simulations focus on the new MPC strategy for the current loop and its dynamical properties; we chose to refrain from showing the behavior of the whole system, to not obstruct
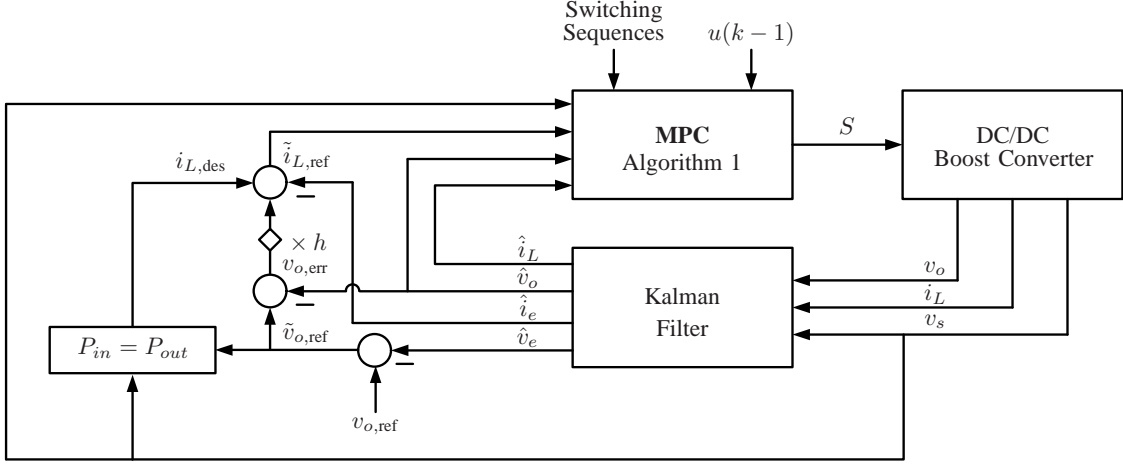
Fig. 6. Control diagram of the proposed MPC strategy.

---

**Algorithm 1** MPC algorithm

> **function** $u^*(k) = \text{MPC}\,(\hat{x}(k), u(k-1))$
>   $J_\dagger^*(k) = \infty;\ u^*(k) = \emptyset;\ x(k) = \hat{x}(k)$
>   **for** all $U$ over $N$ **do**
>     $J_\dagger = 0$
>     **for** $\ell = k$ to $k + N - 1$ **do**
>       $x(\ell+1) = f_\dagger(x(\ell), u(\ell))$
>       $i_{L,\mathrm{err},\dagger}(\ell) = g_\dagger(x(\ell), x(\ell+1))$
>       $\Delta u(\ell) = u(\ell) - u(\ell-1)$
>       $J_\dagger = J_\dagger + i_{L,\mathrm{err},\dagger}(\ell) + \lambda |\Delta u(\ell)|^p$
>     **end for**
>     **if** $J_\dagger < J_\dagger^*(k)$ **then**
>       $J_\dagger^*(k) = J_\dagger,\ u^*(k) = U(1)$
>     **end if**
>   **end for**
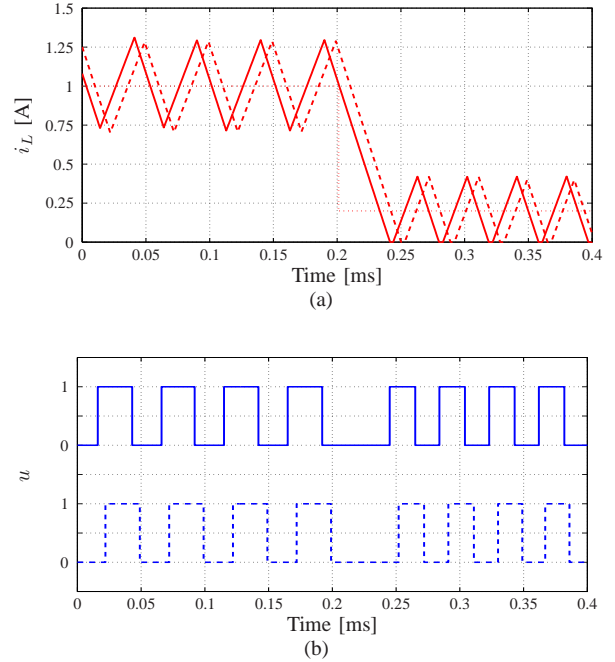> **end function**



(a)



(b)

Fig. 7. Simulation results for the step-down change scenario: a) inductor current for the first (average current error-based—solid line) and the second (rms current error-based—dashed line) approach, along with the inductor current reference (dotted line), b) pulses for the first (solid line) and the second (dashed line) approach.

the dynamical analysis. Thus, for both approaches the same scenario is examined, namely a step-down change in the inductor current reference. The behavior of the converter in both CCM and DCM is examined.

The circuit parameters are $L = 450\,\mu\mathrm{H}$, $R_L = 0.3\,\Omega$ and $C_o = 220\,\mu\mathrm{F}$. The load resistance is assumed to be known and constant for all operating points; it is equal to $R = 73\,\Omega$. Initially, the input voltage is $v_s = 10\,\mathrm{V}$, while the output reference voltage is set equal to $v_{o,\mathrm{ref}} \approx 26.6\,\mathrm{V}$, corresponding to the reference inductor current $i_{L,\mathrm{ref}} = 1\,\mathrm{A}$. Regarding the objective function, the weighting factor is tuned in such a way that the switching frequency in both approaches is approximately the same, i.e. $\lambda = 0.2$ for the first approach and $\lambda = 0.4$ for the second. The prediction horizon is $N = 5$, and the sampling interval is $T_s = 2.5\,\mu\mathrm{s}$.

The converter initially operates under nominal conditions. At time $t = 0.2\,\mathrm{ms}$, a change to the inductor current reference from $i_{L,\mathrm{ref}} = 1\,\mathrm{A}$ to $i_{L,\mathrm{ref}} = 0.2\,\mathrm{A}$ occurs. As can be seen in Fig. 7, for both approaches, the inductor current reaches very quickly the new desired level. The switching frequency

is about $f_{sw} \approx 20\,\mathrm{kHz}$. Since the operating points and the corresponding switching frequencies are the same in both approaches, the current ripples observed are identical.

The main difference between the two proposed approaches can be observed in Fig. 8, which relates to the converter operating under nominal and steady-state conditions. The impact of varying the weighting factor $\lambda$ is investigated. The corresponding output voltage error, given by

$$v_{o,\mathrm{err}} = \sqrt{\frac{1}{N}\Big(\sum_{k=1}^{N} v_{o,\mathrm{ref}} - v_o(k)\Big)^2}, \qquad (23)$$
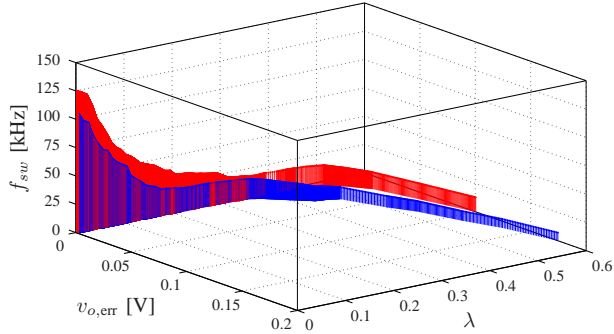
Fig. 8. The output voltage error $v_{o,\text{err}}$ and the corresponding switching frequency $f_{sw}$ versus the weighting factor $\lambda$ for the average current error-based (blue) and the rms current error-based (red) approach when the converter operates under nominal conditions.

and the switching frequency $f_{sw}$ are depicted. As can be seen, the average current error-based approach results in a lower switching frequency with zero tracking error, which means that lower switching losses can be achieved with this approach. On the other hand, the rms current error-based approach leads to higher switching frequencies, when $\lambda$ is very small, due to the quadratic penalty. Such high switching frequencies tend to result in even faster transient responses.

## V. EXPERIMENTAL RESULTS

In order to verify the dynamic behavior of the closed-loop system and to highlight the potential advantages of this novel MPC approach, the control algorithm was implemented on a dSpace real-time system. A boost converter was built using an IRF620 MOSFET and a MUR840 diode as active and passive switches, respectively. The physical values of the circuit parameters are the same as those given in Section IV, i.e. $L = 450\,\mu\text{H}$, $R_L = 0.3\,\Omega$ and $C_o = 220\,\mu\text{F}$. The nominal conditions refer to an input voltage of $v_s = 10\,\text{V}$ and a load resistance of $R = 73\,\Omega$. If not otherwise stated, the output voltage reference is $v_{o,\text{ref}} = 15\,\text{V}$. Hall effect transducers were used to acquire the voltage and inductor current measurements.

The control algorithm was implemented on a dSpace DS1104 real-time system. The proposed MPC strategy is executed every $T_s = 15\,\mu\text{s}$ and a prediction horizon of three steps is used ($N = 3$). The weighting factor in the objective function is set to $\lambda = 0.4$. Depending on the tuning of $\lambda$, both control approaches yield similar results, as shown in the previous section. Therefore, it suffices to present the dynamic behavior of only one methodology. This section focuses on the average current error-based approach. Regarding the Kalman filter, the covariance matrices are chosen as $Q = \text{diag}(0.1, 0.1, 50, 50)$ and $R = \text{diag}(1, 1)$.

### A. Start-up

First, the dynamic behavior of the converter during start-up and nominal conditions is investigated. As can be seen in Fig. 9(b), the inductor current quickly increases in order to charge the capacitor to the desired voltage level. The
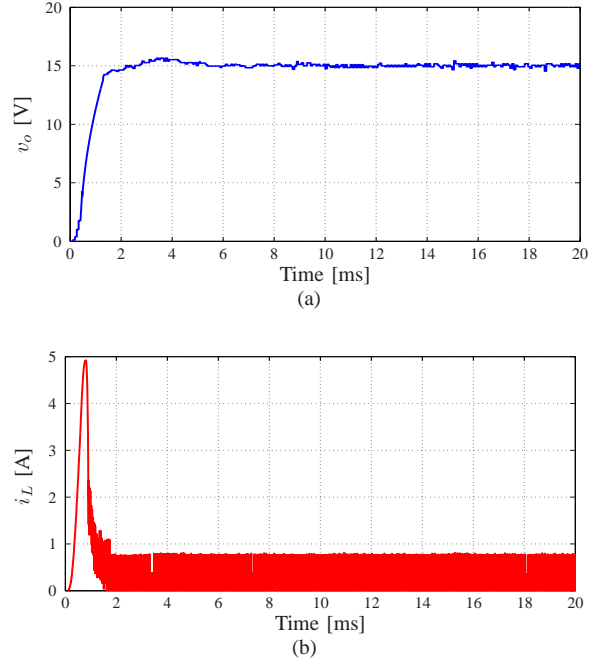


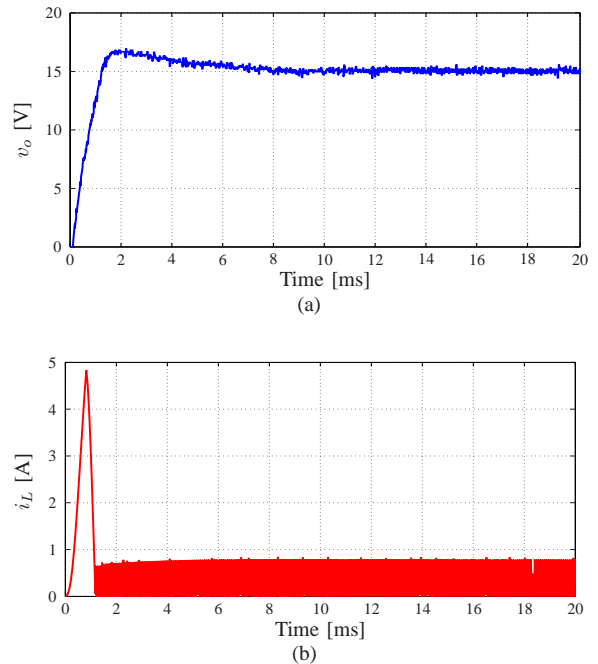Fig. 9. Experimental results for nominal start-up with MPC: a) output voltage, and b) inductor current.



Fig. 10. Experimental results for nominal start-up with a PI controller: a) output voltage, and b) inductor current.

output voltage reaches its reference in $t \approx 3\,\text{ms}$ with a small overshoot, see Fig. 9(a). After the transient, the inductor current reaches its nominal value and the converter operates in DCM.

For comparison purposes, a conventional proportional-integral (PI) controller has been implemented, using the same outer loop as MPC. The respective voltage and current wave-
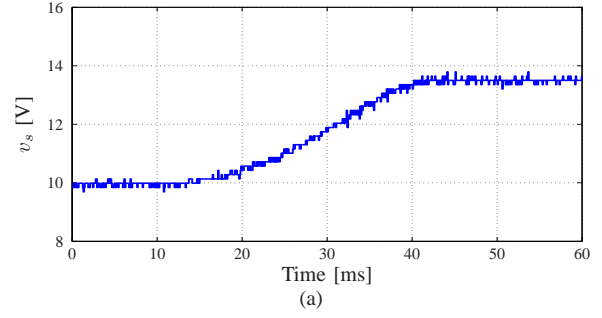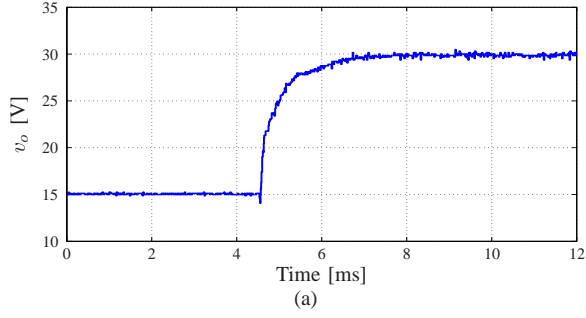
Fig. 11. Experimental results for a step-up change in the output voltage reference with MPC: a) output voltage, and b) inductor current.
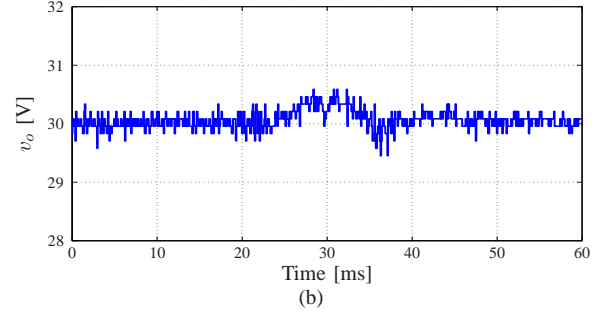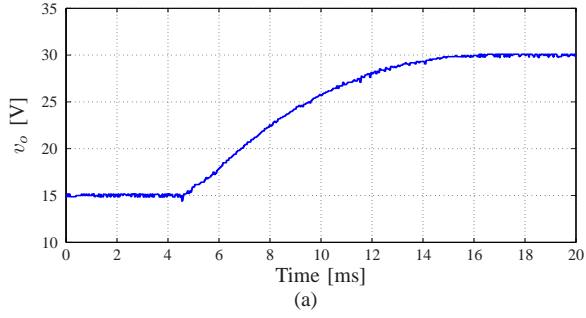


Fig. 12. Experimental results for a step-up change in the output voltage reference with a PI controller: a) output voltage, and b) inductor current.

forms are depicted in Fig. 10. As can be seen, the overshoot in the output voltage in Fig. 10(a) results in a significantly longer settling time compared to MPC of about $t \approx 8\,\text{ms}$.

*B. Step Change in the Output Reference Voltage*

Next, a step-up change in the reference of the output voltage is considered. At time instant $t \approx 4.5\,\text{ms}$ the output voltage
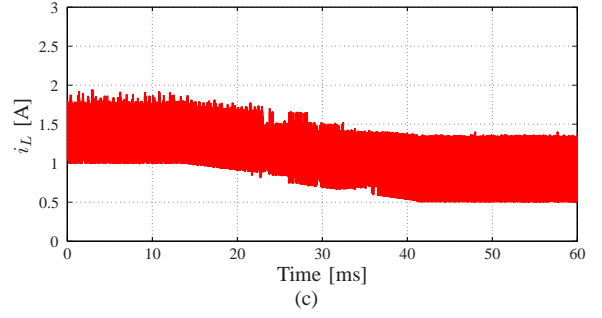


Fig. 13. Experimental results for a ramp change in the input voltage with MPC: a) input voltage, b) output voltage, and c) inductor current.

reference steps up from its initial value, i.e. from $v_{o,\text{ref}} = 15\,\text{V}$ to $v_{o,\text{ref}} = 30\,\text{V}$, see Fig. 11. As previously, the inductor current rapidly increases (Fig. 11(b)) so as to charge the capacitor to the new desired level. Initially, the output voltage briefly decreases due to the non-minimum phase characteristic of the system, before it increases, see Fig. 11(a), reaching its reference value without an overshoot occurring. The transient lasts for about $t \approx 3.5\,\text{ms}$.

On the other hand, when a PI controller is employed, the settling time increases as can be seen in Fig. 12. When the step-up change in the reference voltage occurs at $t \approx 4.5\,\text{ms}$, the current does not significantly increase to quickly charge the capacitor to the new desired level (Fig. 12(b)). Thus, the output voltage reaches its new demanded value in about $t \approx 10\,\text{ms}$, see Fig 12(a).

*C. Ramp Change in the Input Voltage*

For the third case, a ramp change in the input voltage is imposed, starting at $t \approx 16\,\text{ms}$ and lasting until $t \approx 38\,\text{ms}$, as can be seen in Fig. 13(a). The input voltage is manually

Fig. 15. Experimental results for a step change in the load with MPC: a) output voltage, and b) inductor current.
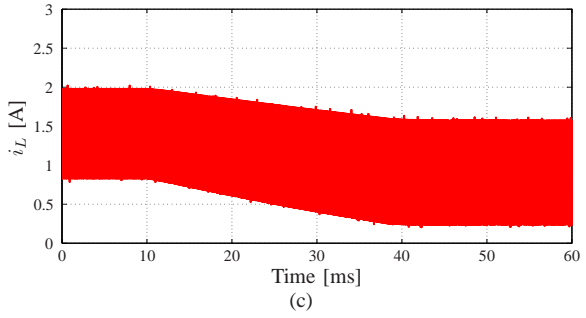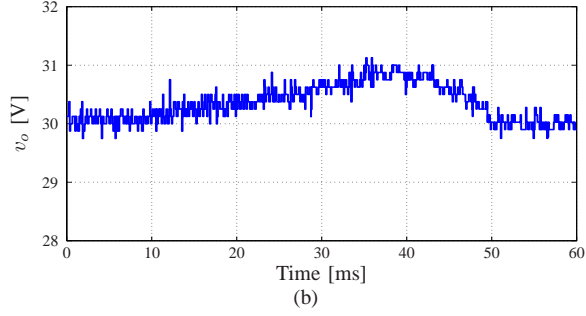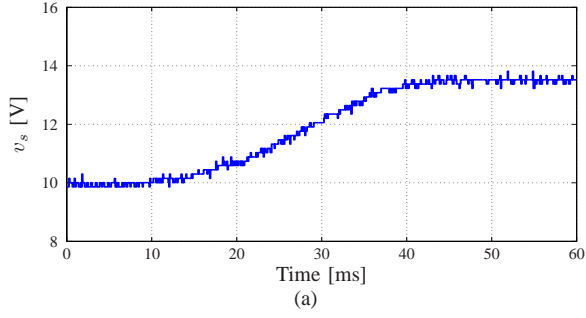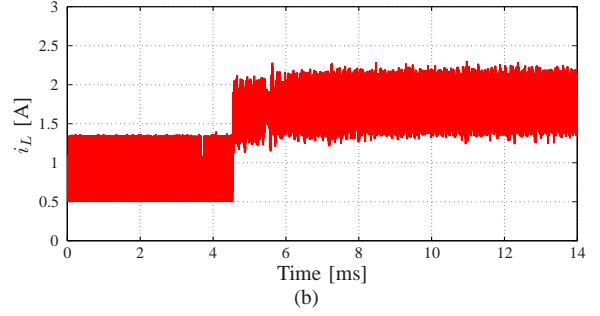


Fig. 14. Experimental results for a ramp change in the input voltage with a PI controller: a) input voltage, b) output voltage, and c) inductor current.

increased from $v_s = 10\,\mathrm{V}$ to $v_s = 13.5\,\mathrm{V}$, while the output voltage reference is $v_{o,\mathrm{ref}} = 30\,\mathrm{V}$. The effects on the output voltage and the inductor current are shown in Figs. 13(b) and 13(c), respectively. During this interval, the inductor current decreases until it reaches its new nominal value. The output voltage is not affected by the change in the input voltage and remains equal to its reference value.

The dynamical behavior of the system is examined under the same conditions when controlled by a PI controller. At $t \approx 10\,\mathrm{ms}$, the input voltage starts to increase until $t \approx 40\,\mathrm{ms}$, when it reaches its final value $v_s = 13.5\,\mathrm{V}$. The system response is depicted in Fig. 14, showing that the PI controller requires about $t \approx 10\,\mathrm{ms}$ to eliminate the steady-state error.

*D. Load Step Change*

Finally, a step-down in the load resistance is examined. At $t \approx 4.5\,\mathrm{ms}$ the load resistance is halved, from its nominal value of $R = 73\,\Omega$ to $R = 36.5\,\Omega$. In Fig. 15 the closed-loop performance of the converter is depicted. The Kalman filter adjusts both the output voltage and the inductor current
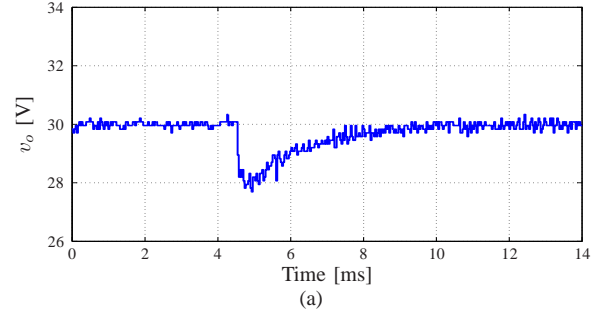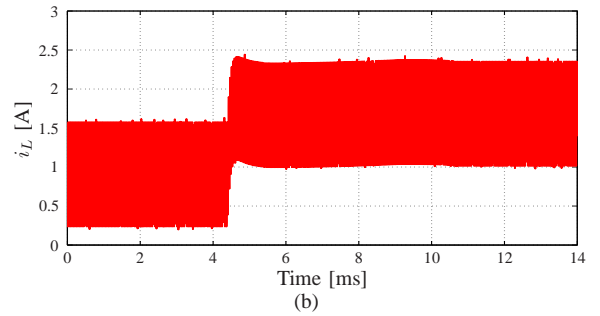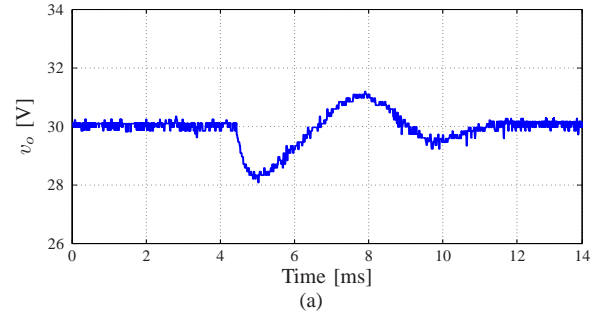


Fig. 16. Experimental results for a step change in the load with a PI controller: a) output voltage, and b) inductor current.

references. The average value of the current is instantaneously doubled, see Fig. 15(b), while a small undershoot in the output voltage is observed during the transient, see Fig. 15(a). When the converter reaches steady-state operation, a zero steady-state error is achieved thanks to the integrating character of the Kalman filter.

However, when a PI controller is used, the transient lasts

longer and the voltage response is weakly dampened, indicating that the tuning of the PI controller is fairly aggressive, see Fig. 16. The load resistance is stepped down at $t \approx 4.5$ ms, while the converter settles at the new operating point after about $t \approx 7$ ms.

## VI. CONCLUSION

In this paper, two different MPC approaches based on enumeration were introduced for the dc-dc boost converter. The implementation of MPC as a current controller (rather than a voltage controller) enables the use of a relatively short prediction horizon, requiring less computational power. In addition, an adequate estimation scheme based on a Kalman filter was implemented in order to address model uncertainties. The performance of the proposed methods are compared via simulations. Both MPC approaches yield a similar behavior during transients, with very fast dynamics. Moreover, experimental results—for the average current error-based approach—are provided, validating the effectiveness of the proposed controller and a high degree of robustness to parameter variations. These benefits outweigh the drawbacks, which arise from the variable switching frequency.

## REFERENCES

[1] T. Geyer, G. Papafotiou, and M. Morari, "Model predictive control in power electronics: A hybrid systems approach," in *Proc. IEEE Conf. Decis. Control*, Seville, Spain, Dec. 2005, pp. 5606–5611.

[2] J. M. Maciejowski, *Predictive Control with Constraints*. Englewood Cliffs, NJ: Prentice-Hall, 2002.

[3] J. B. Rawlings and D. Q. Mayne, *Model Predictive Control: Theory and Design*. Madison, WI: Nob Hill, 2009.

[4] P. Correa, M. Pacas, and J. Rodríguez, "Predictive torque control for inverter-fed induction machines," *IEEE Trans. Ind. Electron.*, vol. 54, no. 2, pp. 1073–1079, Apr. 2007.

[5] H. Miranda, P. Cortés, J. I. Yuz, and J. Rodríguez, "Predictive torque control of induction machines based on state-space models," *IEEE Trans. Ind. Electron.*, vol. 56, no. 6, pp. 1916–1924, Jun. 2009.

[6] T. Geyer, G. Papafotiou, and M. Morari, "Model predictive direct torque control—Part I: Concept, algorithm and analysis," *IEEE Trans. Ind. Electron.*, vol. 56, no. 6, pp. 1894–1905, Jun. 2009.

[7] Y. A.-R. I. Mohamed and E. F. El-Saadany, "Robust high bandwidth discrete-time predictive current control with predictive internal model—A unified approach for voltage-source PWM converters," *IEEE Trans. Power Electron.*, vol. 23, no. 1, pp. 126–136, Jan. 2008.

[8] G. H. Bode, P. C. Loh, M. J. Newman, and D. G. Holmes, "An improved robust predictive current regulation algorithm," *IEEE Trans. Ind. Appl.*, vol. 41, no. 6, pp. 1720–1733, Nov. 2005.

[9] P. Cortés, J. Rodríguez, P. Antoniewicz, and M. Kazmierkowski, "Direct power control of an AFE using predictive control," *IEEE Trans. Power Electron.*, vol. 23, no. 5, pp. 2516–2523, Sep. 2008.

[10] J. Rodríguez, J. Pontt, C. A. Silva, P. Correa, P. Lezana, P. Cortés, and U. Ammann, "Predictive current control of a voltage source inverter," *IEEE Trans. Ind. Electron.*, vol. 54, no. 1, pp. 495–503, Feb. 2007.

[11] P. Cortés, A. Wilson, S. Kouro, J. Rodríguez, and H. Abu-Rub, "Model predictive control of cascaded H-bridge multilevel inverters," *IEEE Trans. Ind. Electron.*, vol. 57, no. 8, pp. 2691–2699, Aug. 2010.

[12] S. Bibian and H. Jin, "High performance predictive dead-beat digital controller for dc power supplies," *IEEE Trans. Power Electron.*, vol. 17, no. 3, pp. 420–427, May 2002.

[13] J. Chen, A. Prodić, R. W. Erickson, and D. Maksimović, "Predictive digital current programmed control," *IEEE Trans. Power Electron.*, vol. 18, no. 1, pp. 411–419, Jan. 2003.

[14] Y. T. Chang and Y. S. Lai, "Online parameter tuning technique for predictive current-mode control operating in boundary conduction mode," *IEEE Trans. Ind. Electron.*, vol. 56, no. 8, pp. 3214–3221, Aug. 2009.

[15] J. Xu, G. Zhou, and M. He, "Improved digital peak voltage predictive control for switching dc-dc converters," *IEEE Trans. Ind. Electron.*, vol. 56, no. 8, pp. 3222–3229, Aug. 2009.

[16] Y. Qiu, H. Liu, and X. Chen, "Digital average current-mode control of PWM dc-dc converters without current sensors," *IEEE Trans. Ind. Electron.*, vol. 57, no. 5, pp. 1670–1677, May 2010.

[17] T. Geyer, G. Papafotiou, R. Frasca, and M. Morari, "Constrained optimal control of the step-down dc-dc converter," *IEEE Trans. Power Electron.*, vol. 23, no. 5, pp. 2454–2464, Sep. 2008.

[18] T. Geyer, G. Papafotiou, and M. Morari, "Hybrid model predictive control of the step-down dc-dc converter," *IEEE Trans. Contr. Syst. Technol.*, vol. 16, no. 6, pp. 1112–1124, Nov. 2008.

[19] A. G. Beccuti, G. Papafotiou, R. Frasca, and M. Morari, "Explicit hybrid model predictive control of the dc-dc boost converter," in *Proc. IEEE Power Electron. Spec. Conf.*, Orlando, FL, Jun. 2007, pp. 2503–2509.

[20] A. G. Beccuti, S. Mariéthoz, S. Cliquennois, S. Wang, and M. Morari, "Explicit model predictive control of dc-dc switched-mode power supplies with extended Kalman filtering," *IEEE Trans. Ind. Electron.*, vol. 56, no. 6, pp. 1864–1874, Jun. 2009.

[21] F. M. Oettmeier, J. Neely, S. Pekarek, R. DeCarlo, and K. Uthaichana, "MPC of switching in a boost converter using a hybrid state model with a sliding mode observer," *IEEE Trans. Ind. Electron.*, vol. 56, no. 9, pp. 3453–3466, Sep. 2009.

[22] Y. Xie, R. Ghaemi, J. Sun, and J. S. Freudenberg, "Implicit model predictive control of a full bridge dc-dc converter," *IEEE Trans. Power Electron.*, vol. 24, no. 12, pp. 2704–2713, Dec. 2009.

[23] P. Karamanakos, G. Papafotiou, and S. Manias, "Model predictive control strategies for dc-dc boost voltage conversion," in *Proc. Eur. Power Electron. Conf.*, Birmingham, UK, Aug./Sep. 2011, pp. 1–9.

[24] P. Karamanakos, T. Geyer, and S. Manias, "Direct voltage control of dc-dc boost converters using enumeration-based model predictive control," *IEEE Trans. Power Electron.*, vol. 29, no. 2, pp. 968–978, Feb. 2014.

[25] ——, "Direct model predictive current control of dc-dc boost converters," in *Proc. Int. Power Electron. and Motion Control Conf. and Expo.*, Novi Sad, Serbia, Sep. 2012, pp. DS2c.11–1–DS2c.11–8.

[26] R. W. Erickson and D. Maksimović, *Fundamentals of Power Electronics*, 2nd ed. Norwell, MA: Kluwer Academic, 2001.

[27] A. Bemporad and M. Morari, "Control of systems integrating logic, dynamics and constraints," *Automatica*, vol. 35, no. 3, pp. 407–427, Mar. 1999.

[28] P. Cortés, S. Kouro, B. La Rocca, R. Vargas, J. Rodríguez, J. I. León, S. Vazquez, and L. G. Franquelo, "Guidelines for weighting factors design in model predictive control of power converters and drives," in *Proc. IEEE Int. Conf. Ind. Technol.*, Gippsland, Australia, Feb. 2009, pp. 1–7.

[29] G. Pannocchia and J. B. Rawlings, "Disturbance models for offset-free model-predictive control," *AIChE J.*, vol. 49, no. 2, pp. 426–437, Feb. 2003.